

Title	Fabrication and Applications of Rapidly Quenched Metals
Author(s)	Naka, Masaaki; Shibayanagi, Toshiya
Citation	Transactions of JWRI. 27(1) p.15-p.22
Issue Date	1998-07
oaire:version	VoR
URL	https://doi.org/10.18910/7147
rights	
Note	

Osaka University Knowledge Archive : OUKA

<https://ir.library.osaka-u.ac.jp/>

Osaka University

Fabrication and Applications of Rapidly Quenched Metals†

Masaaki NAKA* and Toshiya SHIBAYANAGI**

Abstract

Rapid quenching techniques of metals and their applications are reviewed with special reference to the effect of cooling rate on the microstructure of metals, and to clarify critical thermodynamic and kinetic criteria for the formation of metastable materials. Rapid quenching from the liquid state brings about, not only the refinement of microstructures, but also many non-equilibrium states such as super-saturated solid solutions containing amounts of solutes other than the equilibrium one, meta-stable crystalline phases and amorphous phases. Formation of non-equilibrium phases such as amorphous phases is explained in terms of thermodynamics and kinetics, and some applications of the rapidly quenched metals are mentioned.

KEY WORDS: (Rapid Quenching)(Cooling Rate)(Amorphous Phase)(Thermodynamics)(Kinetics)

1. Introduction

Rapid quenching of liquid metals has attracted much interest in current fields of materials science and technology, since this technique has succeeded in producing many new non-equilibrium materials including amorphous metals. In the rapid quenching technique the cooling rate, which is an essential factor controlling microstructures, physical and chemical properties of quenched metals, exceeds 10^3 to 10^7 K/s, compared with a maximum cooling rate of 5×10^3 K/s used in conventional steel industries.

Some new phenomena are known to occur in rapidly quenched metals, *i. e.* refinement of microstructure, improvement of chemical homogeneity, extension of solid solubility of alloying elements and formation of metastable phases including amorphous phases.

The rapid quenching techniques were applied for producing several new type of structural materials. For engineering structural materials, rapidly quenched Al alloys with high strength, high toughness and high corrosion resistance were developed for aircraft components in the 1980's¹⁾. Furthermore, amorphous alloys with no crystalline atomic periodicity in the structure were found to show novel physical and chemical properties²⁾³⁾.

This present review summarizes quenching techniques of metals from the liquid states, the effect of cooling rate on

microstructure of metals, and clarifies critical thermodynamic and kinetic criteria for the formation of metastable materials. The work also describes their fundamental properties and engineering applications.

2. Methods of rapid quenching and cooling rate

Figure 1 shows four typical methods of rapid quenching, *i. e.* gas atomization, centrifugal atomization, melt spinning and self-quenching. The gas atomizing method produces fine powders by spraying and quenching molten metals using high pressure gas. The centrifugal atomizing method quenches liquid metals by spraying onto a rotating disk at high speed. The melt spinning method produces thin films or wires by spraying and quenching liquid metals on a roll which is rotating at high speed. The self-quenching method utilizes laser or electron beams which melt the surface region of the alloys followed by self-cooling in the same bulky materials.

Depending on the quenching techniques, the shapes of rapidly quenched metals show a variety of forms such as powders, flakes, films, wires⁴⁾ and modified surface layers.

Cooling rates for gas-atomized small liquid particles were calculated by means of the finite element method, assuming that the solidification starts from the surface of a spherical particle.

† Received on June 1, 1998

* Professor

** Associate Professor

Transactions of JWRI is published by Joining and Welding Research Institute of Osaka University, Ibaraki, Osaka 567-0047, Japan.

Figure 2⁵⁾ shows a comparison of the results of numerical calculation and the experiments. In this figure the measured data were obtained from the dendrite arm

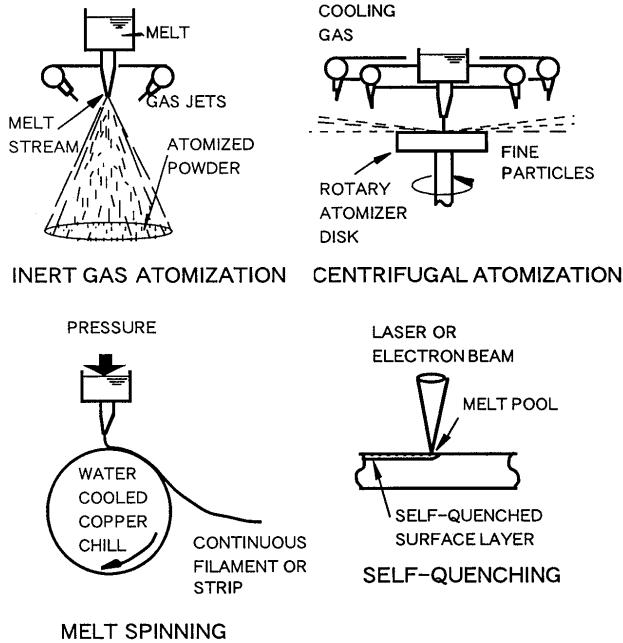


Fig. 1 Four typical methods of rapid solidification processing.

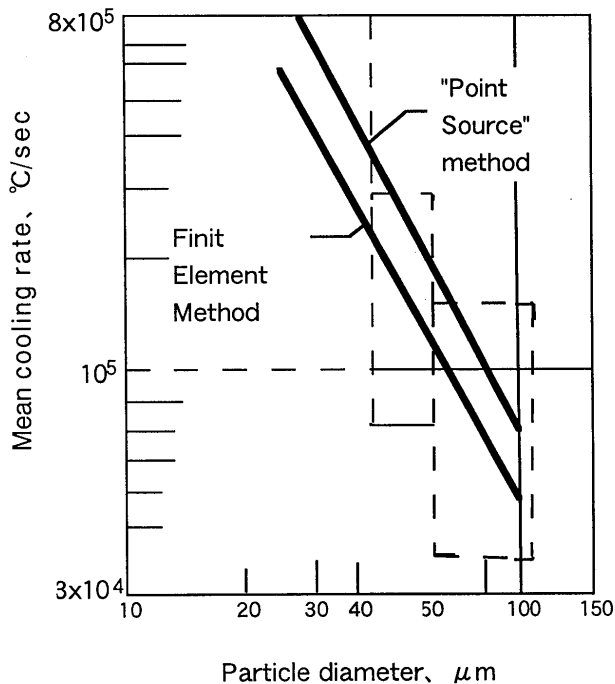


Fig. 2 Comparison of predicted cooling rates with those obtained from measurement of secondary dendrite arm spacings.

spacing, indicating the formation range of gas-atomized liquid particles. Taking into account both calculated and measured data, cooling rates were determined to be 4×10^4 to 3×10^5 K/s.

The cooling rate (R) for a melt-spun ribbon is given by the following equation on assumption of the Newtonian and ideal cooling;

$$R = \frac{h}{C_p \rho t} (T_l - T_0) \quad (1)$$

where, T_l : temperature of melt, T_0 : temperature of solidified metal, C_p : specific heat of melt, ρ : density of melt, t : thickness of solidified metal, h : thermal conductivity.

From this equation the cooling rate depends on the thickness of the ribbon and the value reaches up to 7×10^5 K/s for $100 \mu\text{m}$ in thickness when solidified using copper wheel as shown in Fig.3.

3. Changes of microstructure and formation of phases in rapidly quenched metals

Microstructure in solidified metals is known to vary with cooling rate (= solidification rate) and temperature gradient during solidification, as shown schematically in Fig. 4. Typical microstructures are ; dendritic, cellular (columnar) and planar (or equiaxed) structures.

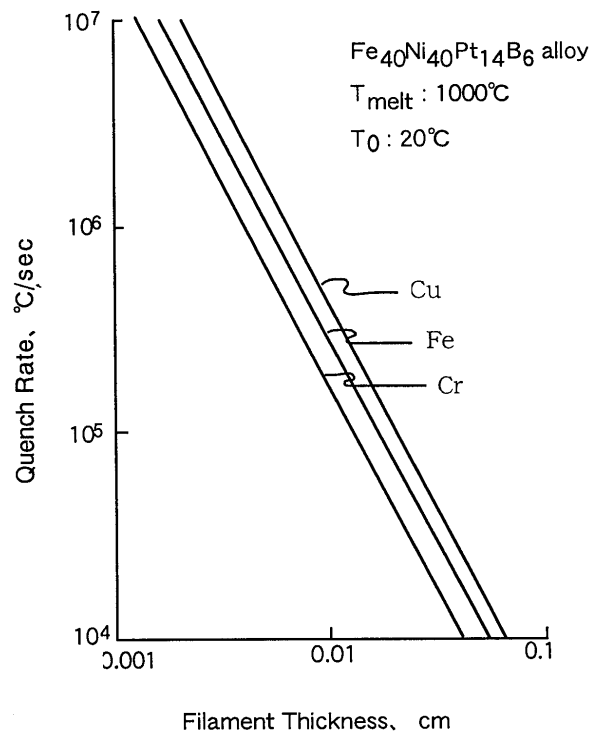


Fig. 3 Relationship of quench rate to filament thickness and substrate character.

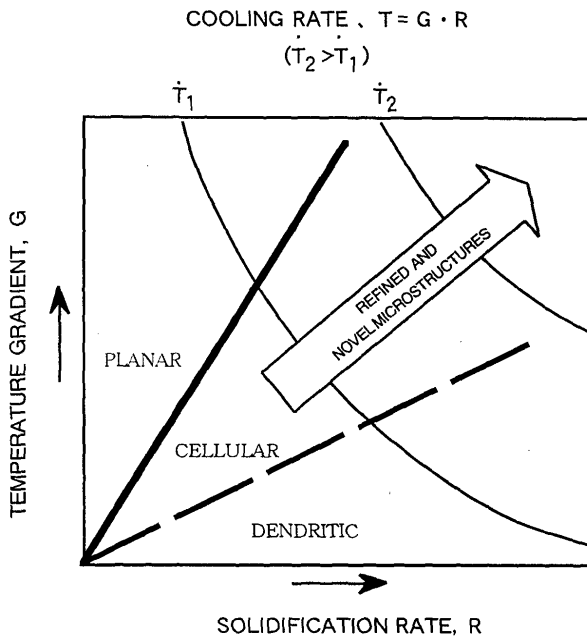


Fig. 4 Dependence of solidification morphology on temperature gradient (G) and solidification rate (R). The qualitative effect of increasing cooling rate is indicated by the sloping arrow.

Refinement of microstructure occurs when the cooling rate from liquid state is increased up to 10²K/s. Dendrite arm spacing(d) is a function of solidification time (ts) and/or average cooling rate (Vav) as follows⁷⁾;

$$d = aV_{av}^{-n} = bt_x^n \quad (2)$$

$$V_{av} = \frac{\Delta T}{t_s} \quad (3)$$

where, ΔT is the temperature range of solidification, and a,b,n are constants.

Figure 5 shows the dependence of secondary dendrite arm-spacing on the cooling rate in Al-4.5mass%Cu alloy⁴⁾, indicating good correlation in the wide range from 10⁵ to 10³ Ks with the coefficient n equal to 0.39. Similar relationships have been reported in many engineering materials such as INNOCENT 718 and maraging steel etc.

The formation of fine columnar structures occurs when solidification proceeds at a larger cooling rate more than 10⁵ K/s which is obtained in the melt spinning method⁸⁾. Melt spinning methods produce under-cooling from melting points of the metals at the interface contacting to the "cooling plane". In this case the initial grain size (d) is related to the growth rate of crystals (U) and the frequency of heterogeneous nucleation (I_g), and the relationship is described by the following equation (4) as;

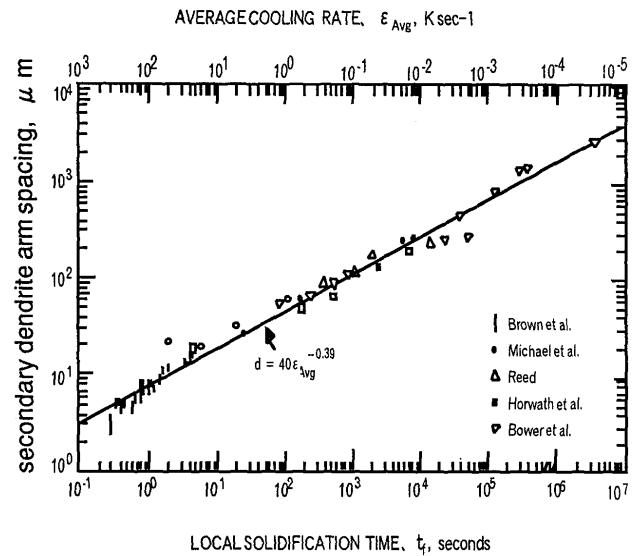


Fig. 5 Relationships of average cooling rate during solidification and secondary dendrite arm spacings in Al-4.5%Cu alloy.

$$d = \left(\frac{8U}{\pi I_c} \right)^{1/3} \quad (4)$$

As the solidification time (ts) is correlated to the rotation rate (V) of coolant by the function as $T_s \propto 1/V$, equation (5) is deduced as ;

$$d/U \propto 1/V \quad (5)$$

Suppose U to be constant, d is proportional to the inverse of Vav. Thus,

$$d \propto 1/V \propto 1/V_{av} \quad (6)$$

Figure 6 shows the relationships between the mean grain size and the inverse of cooling rate investigated for several alloys, and equation (6) can describe these relationships.

Figure 7⁹⁾ shows microstructural changes due to the solidification rate observed for Al-Mn alloys. For example, Al-5mass%Mn alloy changes its microstructure with increasing solidification rate as follows ; primary Al₆Mn needles → fully eutectic → dendritic primary α solid solution → cellular primary α solid solution → α solid solution. In other words, solidification rates larger than 100mm s⁻¹ yield a super saturated solid solution containing more solute atoms than the equilibrium one.

Figure 8¹⁰⁾ shows the extension of solubility in Al-X binary alloys, where the extended region of concentration is indicated by shaded areas. Among these elements, Fe, Co and Ni exhibit highest solubility of several at%, which is two orders of magnitude higher than the equilibrium solubility.

Drastic changes of microstructure are known to occur in some alloys when the cooling rate increases to 10^6 K/s; that is the formation of an amorphous phase possessing no periodicity in atomic configuration. **Figure 9**¹¹⁾ shows the results of TEM observation (bright field images and diffraction patterns) of Metal-P eutectic binary

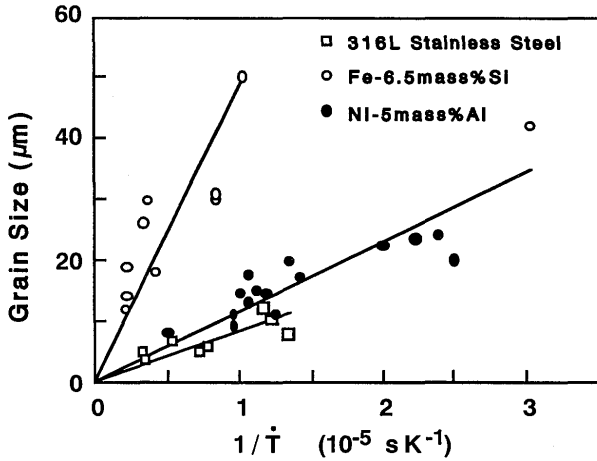


Fig. 6 Grain size in melt-spun ribbons plotted as a function of inverse cooling rate.

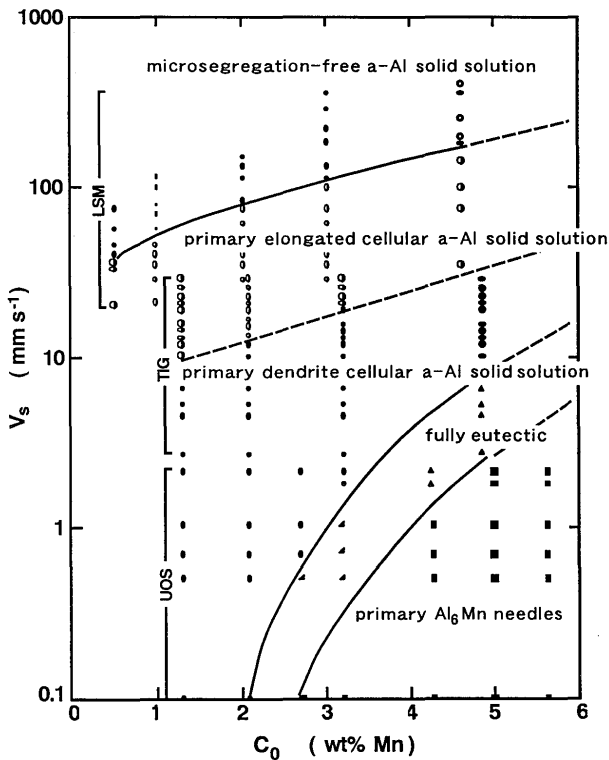


Fig. 7 Solidification microstructure selection diagram for aluminium-rich Al-Mn alloys derived from experimental results of Bridgman, TIG and laser melt traversing.

alloys produced by the melt spinning method. Amorphous phases are observed for Fe-P, Ni-P, Pd-P and Pt-P alloys, while no amorphization occurs in Mn-P, Co-P and Cu-P alloys. In this regard, the formation of an amorphous phase depends on the kind of alloy, and the criterion for this phenomenon will be described in the following section.

Figure 10¹⁾ shows, schematically, the changes in microstructure depending on the cooling rate as mentioned

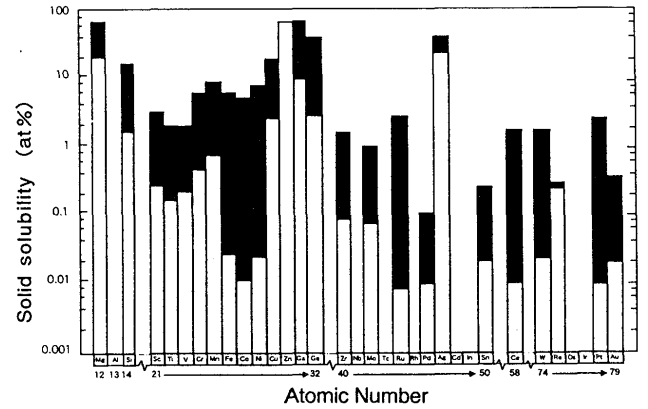


Fig. 8 Solid solubility extension in aluminium as a function of solute atomic number. Lower bound of black bar indicates maximum equilibrium solid solubility while upper boundary indicates extended limit.

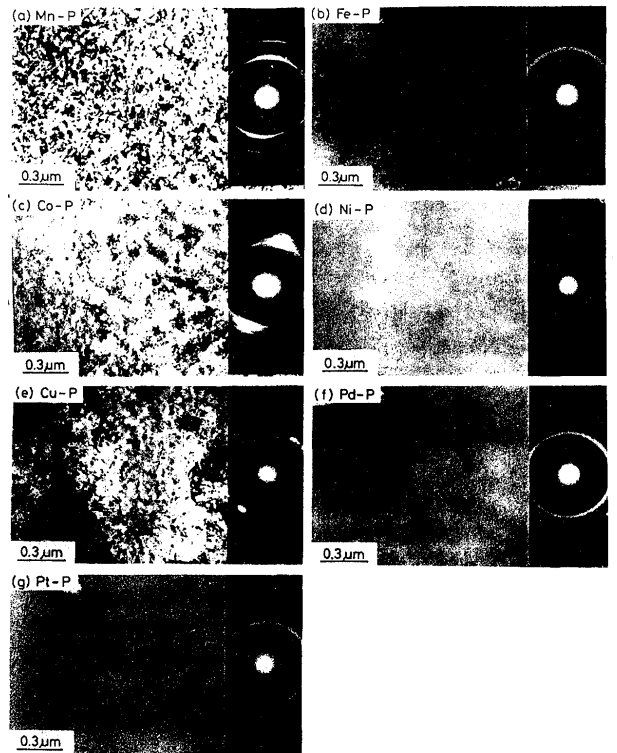


Fig. 9 TEM micrographs (bright field images) and corresponding selected area diffraction patterns of metals-P alloys rapidly solidified.

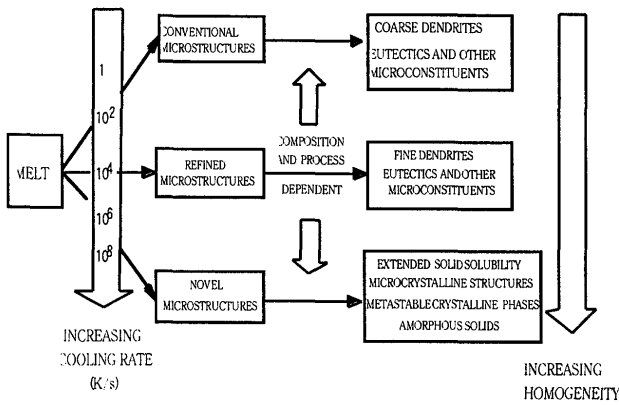


Fig. 10 Microstructural consequences of rapid solidification.

above. An increase in the cooling rate results in a refinement of dendritic or eutectic structures, and the formation of supersaturated solid solutions, metastable crystalline phases, amorphous phases and also quasi-crystals¹²⁾ occurring at higher cooling rates.

4. Formation of metastable phases

Formation of meta-stable phases by rapid quenching from the liquid state is explained in terms of the concept of hierarchy of free energy of each phase which is shown in Fig. 11.

Rapid quenching brings about super-cooling leading to a suppression of crystallization of an equilibrium phase a. Meta-stable phases b and g are formed when the super-cooling reaches and , respectively. Finally, transition of the liquid state into the amorphous state

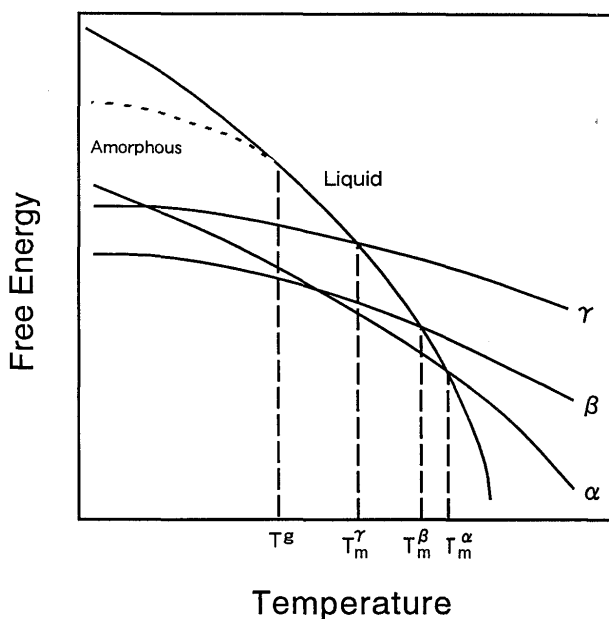


Fig. 11 Hierarchy of free energies in alloys.

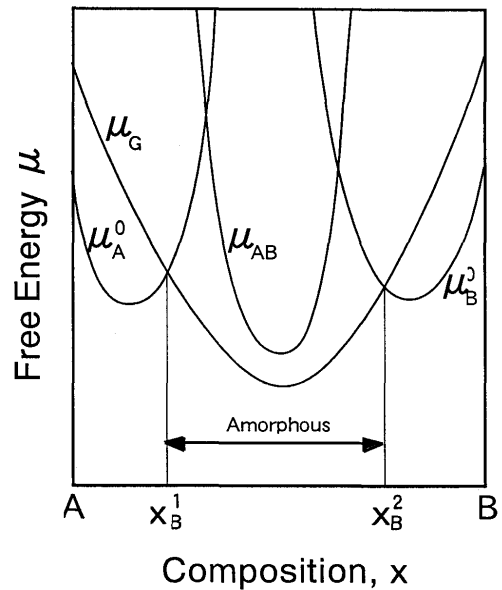


Fig. 12 Gibbs free energy diagram for each phase and amorphous phase in binary alloy.

takes place under further super-cooling conditions where the temperature is below the glass transition temperature (T_g).

In addition, the Gibbs free energy of the alloy is used to explain the compositional dependence of the formation of super-saturated solid solution and amorphization depending on composition.

Figure 12 shows schematically the free energy curves of an alloy at a given temperature below the glass transition temperature. In this figure, x_B^1 and x_B^2 are points of intersection of the free energy locus (μ_G) of the amorphous phase and those of crystals A (μ_A) and B (μ_B), respectively. Crystalline states of A and B are stable and their super-saturated solid solutions are formed in the ranges from pure A to x_B^1 , and from x_B^2 to pure B, respectively. In the range between x_B^1 and x_B^2 , the amorphous phase becomes stable if μ_G is lower than the free energy (μ_{AB}) of intermediate phase AB. In other word, the amorphous phase can be formed in the composition range between x_B^1 and x_B^2 . The amorphous forming range in the free energy - composition diagram of Cu-Zr system is shown in Fig. 13.

Although the above discussion was focused on the thermodynamics of the criterion for amorphization, we need to think about the critical cooling rate for the formation of the amorphous phase, which will be described hereafter based on the theory of nucleation and kinetics of crystal growth from the liquid.

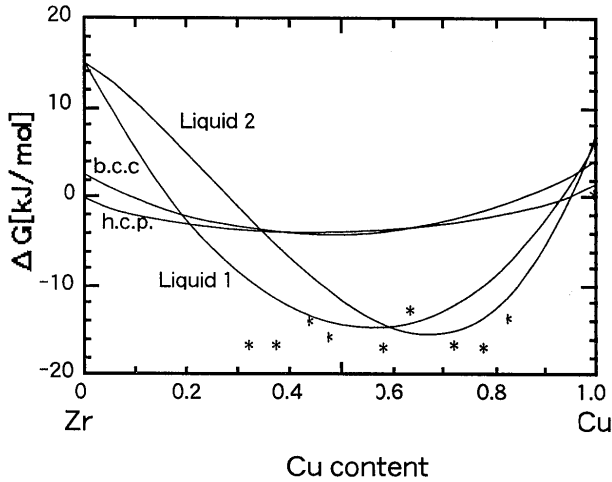


Fig. 13 The free energy of the metastable and equilibrium phases at $T=340^{\circ}\text{C}$. The free energies of hcp zirconium and fcc copper are chosen as reference points. * means free energy of the intermetallic compounds.

Supposing that crystals can nucleate and grow homogeneously in a liquid. Then the volume fraction of the crystals is given by the following equation ;

$$X = \frac{\pi}{3} IU^3 t^4 \quad (7)$$

where I : frequency of homogeneous nucleation, U : growth rate of crystals and t : solidification time.

I is given by the following equation ;

$$I = \frac{N_v D}{a^3} \exp(-G^*/kT) \quad (8)$$

where, N_v : number of atoms in unit volume, D : average diffusion coefficient at the interface between liquid and nuclei of crystal, a : radius of atom and ΔG^* : free energy change for the formation of nuclei with critical radius.

In the case of an amorphous forming system, $\Delta G^*/kT$ is approximated to be $1.07 \sqrt{\Delta T_r^3 \cdot \Delta T_r^2}$.

Meanwhile, U is given by the following equation:

$$U = \frac{fD}{a} [1 - \exp(-\Delta T_r \Delta H/kT)] \quad (9)$$

where, f and H are volume fraction of nucleation site and molar latent heat for fusion, respectively. D is estimated by assuming the Stokes-Einstein's equation and is given as $D = kT/3\pi a\eta$.

where η is the viscosity of super-cooled liquid.

From equations (7), (8) and (9), one can estimate the incubation time (t) for crystallization from the liquid state. From these discussions, the important factor for the formation of an amorphous phase is the viscosity of the liquid, and amorphization occurs at small cooling rates

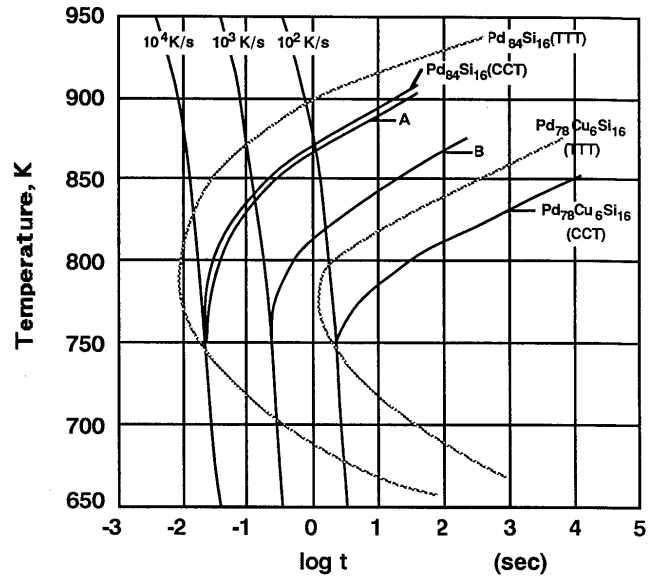


Fig. 14 CCT and TTT curves for $\text{Pd}_{84}\text{Si}_{16}$ and $\text{Pd}_{78}\text{Cu}_6\text{Si}_{16}$ alloys corresponding to a volume fraction crystallized of 10^{-6} .

under the conditions of low T_m and large η values.

The viscosity of a super-cooled liquid is calculated by applying the data of viscosity above T_m and $\eta=10^{13}$ poise at T_g and using Vogel-Fulcher's approximation for a super-cooled liquid given by equation (10);

$$\log \eta = A + B/(T_r - T_0) \quad (10)$$

Figure 14 shows the T-T-T and C-C-T diagram¹⁴⁾ for crystallization from the liquid in the case when $X=10^{-6}$, calculated using the data of viscosity of Pd-Si and Pd-Cu-Si alloys. The critical cooling rate for amorphization is equal to the cooling rate at the nose of the C-C-T curve.

The critical cooling rate of amorphization in Pd-6at%Cu-16at%Si alloy is 10^2 K/s, suggesting that the alloy easily forms amorphous phase under air cooling conditions.

Table 1¹¹⁾ shows the critical cooling rate for amorphization calculated for some Metal-P binary alloys. R_c and R_c^* are the results calculated by Naka et al¹¹⁾ and Davis et al¹⁵⁾, respectively. Taking into account the results shown in Fig.9, the cooling rate is estimated to be 5×10^9 K/s, and this result is consistent with the fact that the amorphization is observed to take place in Fe-P, Ni-P, Pd-P and Pt-P alloys when the critical cooling rates are less than 5×10^9 K/s.

5. Applications of rapidly quenched metals

Rapidly quenched powders contain super-saturated solute atoms and have microstructures with quite small grain sizes. Utilization of these powders enables the

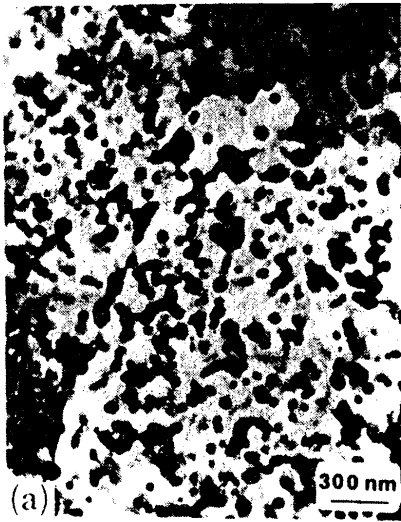


Fig. 15 A typical microstructure of extruded AlFe alloy.

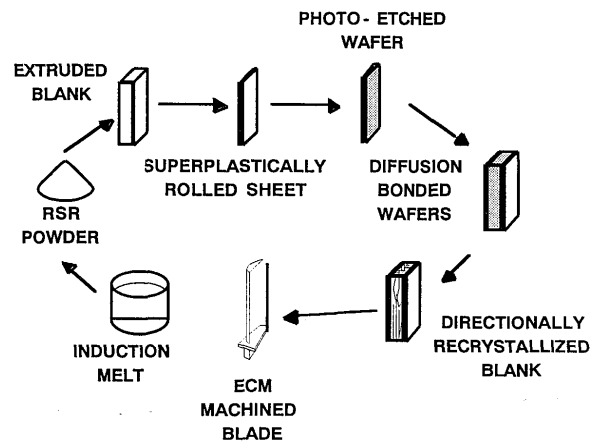
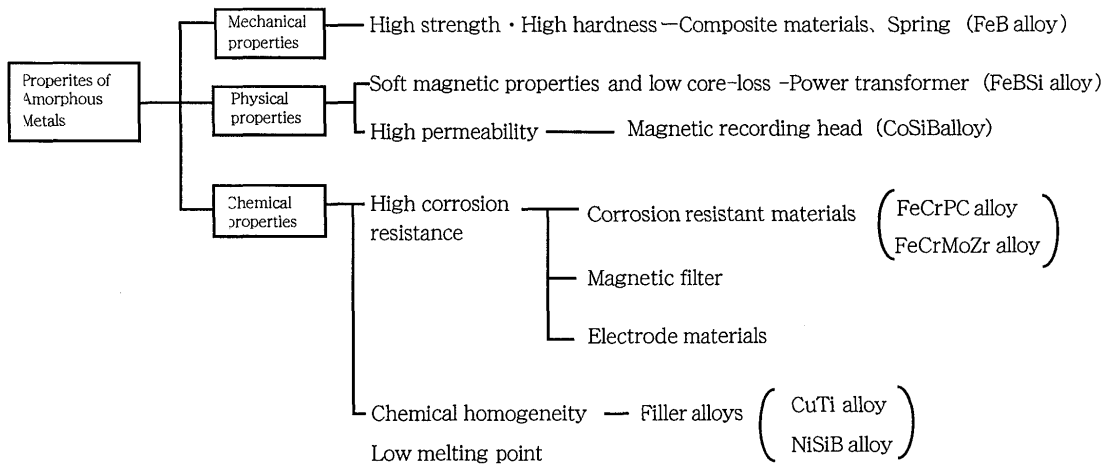


Fig. 16 Sequence of steps in the fabrication of a wafer blade

Table 1 Critical cooling rate for amorphization of metal-P binary alloys

Alloy	Rc (K/s)	Rc* (K/s)
Mn _{86.9} P _{13.1}	2.0 × 10 ⁵	
Fe _{82.5} P _{17.5}	4.6 × 10 ⁶	3.2 × 10 ⁶
Co _{80.1} P _{19.9}	1.4 × 10 ⁷	
Ni ₈₁ P ₁₉	6.3 × 10 ⁵	7.9 × 10 ⁵
Cu _{83.9} P _{16.1}	7.4 × 10 ⁷	
Pd ₈₁ P ₁₉	5.4 × 10 ⁵	2.0 × 10 ⁵
Pt ₈₀ P ₂₀	3.3 × 10 ⁵	6.3 × 10 ⁵

Table 2 Properties and applications of amorphous alloys



equilibrium phase to be dispersed more finely compared with other materials produced by conventional processes. Therefore, these powders are important materials for producing many parts of the frames of aircraft.

Figure 15 shows a typical microstructure of Al-6Fe alloy containing fine particles of FeAl dispersed in the matrix ¹⁶⁾. Ni alloys containing fine Ni₃Al particles as a dispersive are produced in the process which includes the rapid quenching from the liquid state as shown in **Fig. 16**, and used as heat resistant turbine blades of jet-engines in aircraft.

Amorphous alloys show novel characteristics in mechanical, physical and chemical properties as summarized in **Table 2**, and several applications of these alloys have been proposed. Amorphous phases are also taken as a matrix for the development of new materials such as magnetic materials ¹⁷⁾ containing nano-crystalline phases in an amorphous matrix, or high strength Al alloys ¹⁸⁾.

6. Summary

Rapid quenching from the liquid state brings about not only the refinement of microstructures but also many non-equilibrium states such as super-saturated solid solution containing amount of solutes other than the equilibrium one, meta-stable crystalline phases and amorphous phases.

Formation of these phases is explained by the hierarchy of the free energy of the formation of each phase and the nucleation and growth process of crystals from the liquid phase. Meta-stable phases exhibits novel characteristics in physical, chemical and mechanical properties which are not attained by conventional materials, and some new uses of these meta-stable phases are now being introduced in many engineering fields.

REFERENCES

- 1) M.Cohen, B.H.Keah and R.Mehrabian, Proc. 2nd. Int. Conf. on Rapid Solidification Processing, Claiter's Pub., (1980), 1—23.
- 2) T.Masumoto, Proc. 4th Int. Conf. on Rapidly Quenched Metals, J.Japan Inst. Metals, (1981), 5-10.
- 3) M.Naka, T.Hashimoto and T.Masumoto : J.Japan Inst. Metals, 38(1974),835—841.
- 4) I.Ohnaka, T.Fukusako : Proc. 4th. Int. Conf. on Rapidly Quenched Metals, J.Japan Inst. Metals, (1981), 31-34.
- 5) M.R.Glickastein, R.T.Patterson and N.E.Shockey : Proc. Int. Conf. on Rapid Solidification Processing, 1977, 46—63.
- 6) S.Kavesh : Proc. Int. Conf. on Rapid Solidification Processing, (1977), 165—187.
- 7) R.Mehrabian : Proc. Int. Conf. on Rapid Solidification Processing, (1977), 9—27.
- 8) A.L. Greer : Pro. 7th Int. Conf. on Rapidly Quenched Metals, Elsevier Sci. Pub., (1990), 16—21.
- 9) H.Jones : Pro. 7th Int. Conf. on Rapidly Quenched Metals, Elsevier Sci. Pub., (1990), 33—39.
- 10) S.P.Midson and H.Jones : Pro. 4th Int. Conf. on Rapidly Quenched Metals, J.Japan Inst. Metals, (1982), 1539—1544.
- 11) M.Naka, A.Inoue and T.Masumoto : Sci. Rep. Res. Inst. Tohoku Univ., A29(1981), No.2, 194—194.
- 12) D.Shechtman, I.Blech, D.Gratias and J.W.Cahn, Phys. Rev. Lett., 53(1984), 1951—1954.
- 13) R.Bormann, F.Gaertner and F.Haider : Proc. 6th Int. Conf. on Rapidly Quenched Metals, Elsevier Applied Science, (1987), 79—81.
- 14) M. Naka, Y.Nishi and T.Masumoto : Proc. 3rd Int. Conf. on Rapidly Quenched Metals, The Metals Soci., (1978), 231—238.
- 15) H.A.Davis and B.C.Lewis : Scripta Met., 9(1975),1107.
- 16) W.Beak: Proc. 7th Int. Conf. on Rapidly Quenched Metals, Elsevier Sci. Pub., (1991), 1087—1097.
- 17) A.Malcino, T.Hatanai, A.Inoue and T.Masumoto, Pro. 9th Int. Conf. on Rapidly Quenched Metals, Elsevier Sci. Pub., (1997), 594—602.
- 18) T.Masumoto : Proc. 8th Int. Conf. on Rapidly Quenched Metals, Elsevier Sci. Pub., (1994), 8—16.